P-Vector Inverse Method Evaluated Using the Modular Ocean Model (MOM)

Peter C. Chu[1], Chenwu Fan[1] and Wenju Cai[2]

[1]*Naval Postgraduate School, Monterey, CA 93943, U.S.A.*
[2]*CSIRO Division of Atmospheric Research, Aspendale, Victoria, Australia*

Several major inverse methods (Stommel-Schott method, Wunsch method, and Bernoulli method) have been successfully developed to quantitatively estimate the geostrophic velocity at the reference level from hydrographic data. No matter the different appearance, they are based on the same dynamical sophistication: geostrophy, hydrostatic, and potential density (ρ) conservation (Davis, 1978). The current inverse methods are all based on two conservation principles: potential density and potential vorticity ($q = f\partial\rho/\partial z$) and require β-turning. Thus, two necessary conditions can be incorporated into any inverse methods: (1) non-coincidence of potential density and potential vorticity surfaces and (2) existence of vertical turning of the velocity (β-turning.) This can be done using the P-Vector, a unit vector in the direction of $\nabla\rho \times \nabla q$ (Chu, 1994, 1995). The first necessary condition becomes the existence of the P-vector, and the second necessary condition leads to the existence of the P-vector turning in the water column. Along this line, we developed the P-vector inverse method with a pre-requirement check-up. The method was verified in this study using the Modular Ocean Model (MOM) from Pacanowski *et al.* (1991) version of Bryan-Cox-Semtner ocean general circulation model (OGCM), which is based on the work of Bryan (1969). The statistically steady solutions of temperature and salinity from MOM are used as a "no-error data" set for computing absolute geostrophic velocities by the P-vector inverse method. Circulations are similar between the MOM statistically steady solutions and the P-vector solutions. Furthermore, the quantitative analysis shows that this inverse method has capability of picking up the major signal of the velocity field.

1. Introduction

Our understanding of the mid-latitude large-scale ocean circulation has been greatly benefitted by a remarkable set of papers by Stommel and collaborators (Stommel and Schott, 1977; Schott and Stommel, 1978, Beringer and Stommel, 1980), Wunsch and collaborators (Wunsch, 1978; Wunsch and Grant 1982), and Killworth (1986). Their work makes it possible to obtain ocean general circulations from observations of temperature (T) and salinity (S). The physical base for calculating geostrophic velocity from hydrographic data is the thermal wind relation

$$u = u_0 + \frac{g}{f\rho_0} \int_{z_0}^{z} \frac{\partial\hat{\rho}}{\partial y} dz', \qquad (1)$$

$$v = v_0 - \frac{g}{f\rho_0} \int_{z_0}^{z} \frac{\partial\hat{\rho}}{\partial x} dz' \qquad (2)$$

where (u, v), (u_0, v_0) are the geostrophic velocity at any depth z and at a reference depth z_0, $\hat{\rho}$ is the in situ water density, ρ_0 is the characteristic value of the density, and f is the Coriolis parameter, which is a function of latitude. Here the Boussinesq approximation has been used. As mentioned by Olbers *et al.* (1985), the quantities T, S are relatively easy to measure, and in contrast to velocity observations, the climatological signal in the T, S fields is less contaminated by energetic smaller-scale motions induced by eddies and waves. Equations (1) and (2) indicate that the hydrographic data only determine the baroclinic geostrophic currents. The reference velocity (u_0, v_0) still needs to be determined.

Based on the geostrophy, hydrostatic balance, and mass conservation, several major inverse techniques, i.e., the β-spiral method (Stommel and Schott, 1977; Schott and Stommel, 1978), the Wunsch method (Wunsch, 1978), and Bernoulli method (Killworth, 1986) have been successfully developed to quantify the geostrophic velocity at the reference

level (u_0, v_0). We refer reader to an excellent review paper on β-spiral method by Olbers *et al.* (1985). Davis (1978) pointed out that the β-spiral method and the Wunsch method, no matter how different in appearance, are based on the same order of dynamical sophistication and differ from implicit assumptions about the scales of oceanic variability and different definitions of the smooth field to which the dynamical model pertains.

As pointed out by Wunsch and Grant (1982), in determining large-scale circulation from hydrographic data, we can be reasonably confident on the assumptions of geostrophic balance, mass conservation, and no major cross-isopycnal mixing (except water masses are in contact with the atmosphere). The density of each fluid element would be conserved, i.e.,

$$\mathrm{V} \cdot \nabla \rho = 0 \tag{3}$$

where ρ is the potential density. The conservation of potential vorticity equation (Pedlosky, 1986) can be obtained by differentiating (3) with respect to z, using the geostrophic and hydrostatic balance, and including the latitudinal variation of the Coriolis parameter,

$$\mathrm{V} \cdot \nabla q = 0, \quad q = f\frac{\partial \rho}{\partial z}. \tag{4}$$

Use of $f\partial \rho/\partial z$ may induce a small but systematic error into estimation of potential vorticity (Needler, 1986). Equations (3) and (4) indicate that V is perpendicular to both $\nabla \rho$ and ∇q, therefore, the velocity V is parallel to $\nabla q \times \nabla \rho$.

Recently, Chu (1994, 1995) proposed using a unit vector (P-vector)

$$\mathrm{P} = \frac{\nabla \rho \times \nabla q}{|\nabla \rho \times \nabla q|} \tag{5}$$

to obtaining North Atlantic ocean circulation from hydrographic data. The results were quite agreeable with observations. The major purposes of this paper are to demonstrate the benefit of using P-vector in β-spiral method and to evaluate the P-vector method using an ocean general circulation model.

2. Necessary Conditions for the β-Spiral Method

The three-dimensional velocity field can be determined from the density field unless the potential vorticity and density surfaces coincide (Stommel and Schott, 1977). This leads to the first necessary condition for the validity of any inverse methods.

Necessary Condition 1: The potential density surface does not coincide with the potential vorticity surface; i.e.,

$$\nabla \rho \times \nabla q \neq 0. \tag{6}$$

Stommel and Schott (1977) pointed out that because the horizontal component of velocity rotates with depth in the open ocean (β-spiral), absolute velocities can be obtained from observations of the density field alone. Since all the inverse methods are dynamically equivalent, the β-spiral should be satisfied before using any inverse method. This leads to the second necessary condition.

Necessary Condition 2: The velocity (u, v) should have vertical turning (i.e., the β-spiral) in the water column, i.e., the horizontal velocity should change direction with depth

$$\begin{vmatrix} u^{(k)} & v^{(k)} \\ u^{(m)} & v^{(m)} \end{vmatrix} \neq 0 \tag{7}$$

somewhere in the water column. For a given level $z = z_k$, if we cannot find a level z_m such that (7) is satisfied, the inverse method will fail to get velocity at z_k of this water column.

Before using any inverse method, we need to check if these two necessary conditions are satisfied. If one of them is not satisfied, we cannot use any inverse method to obtain the velocity field from the T, S fields for that water column. The next section shows that a recently proposed P-vector concept (Chu, 1994, 1995) can bring the two necessary conditions into the β-spiral method.

3. P-Vector

Existence of a P-vector (5) implies the satisfaction of the **Necessary Condition 1**. This provides the first check point to see if the potential density surface coincides with the potential vorticity surface. If the necessary condition 1 is satisfied, the P-vector lies on the intersection of the potential density and potential vorticity surfaces (Fig. 1).

The relationship between velocity, $V = (u, v, w)$, and $P = (P_x, P_y, P_z)$, is

$$\mathrm{V} = r(x, y, z)\mathrm{P} \tag{8}$$

where r is the proportionality. Applying the thermal wind relation to any two different depths z_k and z_m, shown as in Fig. 2, a set of algebraic equations for determining the parameter r is obtained

$$r^{(k)}P_x^{(k)} - r^{(m)}P_x^{(m)} = \Delta u_{km}$$

$$r^{(k)}P_y^{(k)} - r^{(m)}P_y^{(m)} = \Delta v_{km} \tag{9}$$

which are two linear algebraic equations for $r^{(k)}$ and $r^{(m)}$. Here $r^{(i)} = r(x, y, z_i)$, and

$$\left(\Delta u_{km}, \Delta v_{km}\right) = \frac{g}{f\rho_0} \int_{z_m}^{z_k} \left(\frac{\partial \hat{\rho}}{\partial y}, -\frac{\partial \hat{\rho}}{\partial x}\right) dz'. \qquad (10)$$

As soon as $r^{(k)}$ is obtained, the velocity field can be computed by (8).

If the determinant

$$\begin{vmatrix} P_x^{(k)} & P_x^{(m)} \\ P_y^{(k)} & P_y^{(m)} \end{vmatrix} \neq 0 \qquad (11)$$

the algebraic equations (9) have definite solutions for $r^{(k)}$ ($m \neq k$):
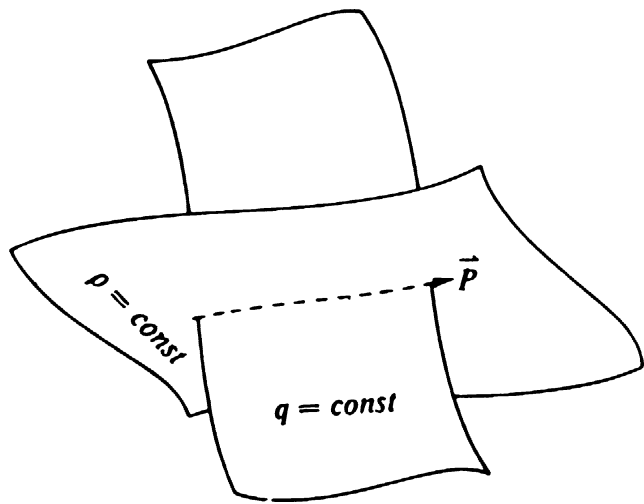

Fig. 1. The absolute velocity and the intersection of the surfaces of potential density and potential vorticity.

$$r^{(k)} = \frac{\begin{vmatrix} \Delta u_{km} & P_x^{(m)} \\ \Delta v_{km} & P_y^{(m)} \end{vmatrix}}{\begin{vmatrix} P_x^{(k)} & P_x^{(m)} \\ P_y^{(k)} & P_y^{(m)} \end{vmatrix}}. \qquad (12)$$

Thus, the P-vector has the second good feature which is the check-up for the β-turning. Consider the P-vector at two different levels, $z = z_k$ and $z = z_m$ (Fig. 2(a)) and use $\boldsymbol{P}_h$, $\boldsymbol{P}_v$ to denote the horizontal and vertical components of the P-vector. The determinant (11) is the sine of the vertical turning angle between $\boldsymbol{P}_h^{(k)}$ and $\boldsymbol{P}_h^{(m)}$ (Fig. 2(b)), i.e.,

$$\begin{vmatrix} P_x^{(k)} & P_x^{(m)} \\ P_y^{(k)} & P_y^{(m)} \end{vmatrix} = \sin\left(\alpha_{km}\right) \qquad (13)$$

where α_{km} indicates the β-spiral turning angle between the two levels z_k and z_m.

In order to use any inverse method, we should check if the inequality (11) holds. If (11) is not satisfied, i.e., the horizontal velocity does not have β-turning,

$$\sin \alpha_{km} = 0, \quad \text{or} \quad P_x^{(m)} = \text{const}, \quad P_y^{(m)} = \text{const},$$
$$\text{for all } m \quad (14)$$

all the inverse methods fail. This is the second necessary condition for checking the β-turning.
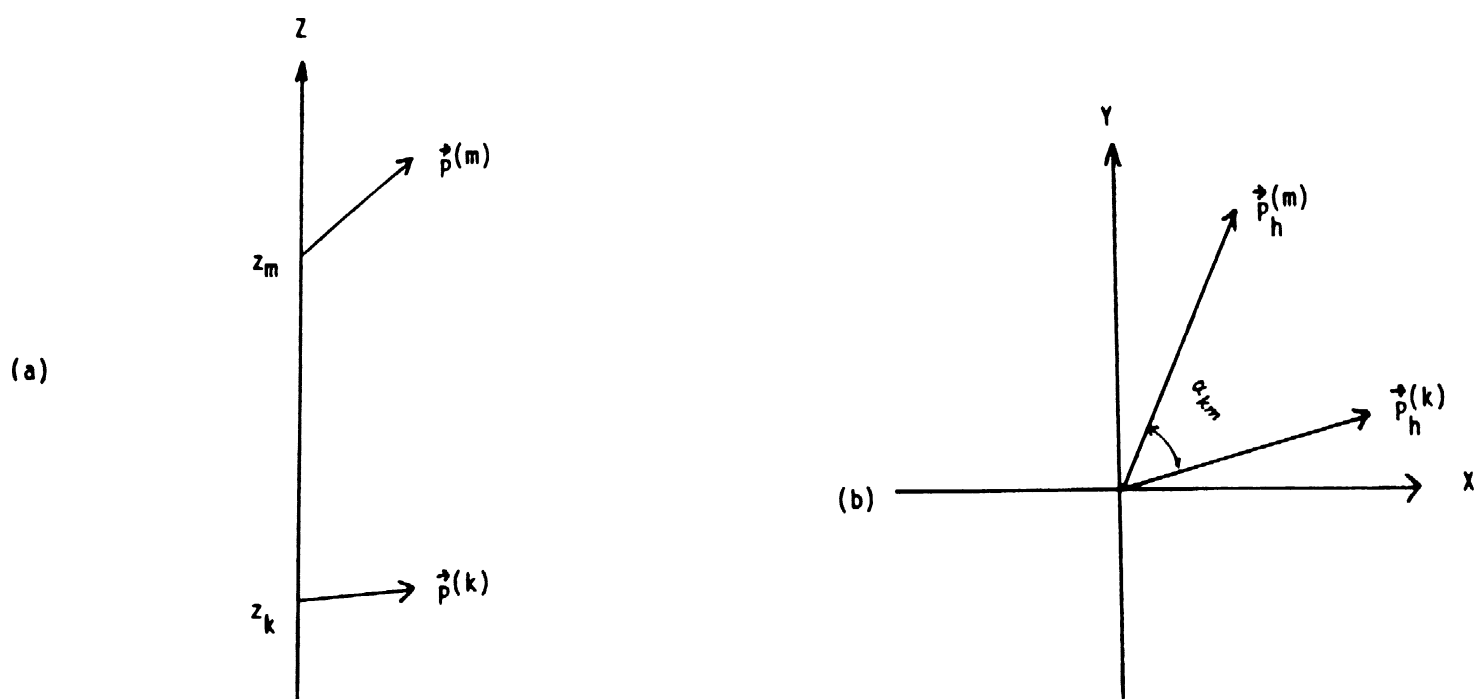

Fig. 2. Vertical turning of the P-vector: (a) P vector at two different levels, and (b) turning angle between two levels (from Chu, 1995).

4. P-Vector Inverse Method

For water columns surviving the two necessary conditions, we may use (12) to compute $r^{(k)}$ for the level z_k. There are $(N-1)$ sets ($m = 1, 2, k-1, k+1, ..., N$) of Eq. (9) for calculating $r^{(k)}$. Here, N is the total vertical levels of the water column. All the $(N-1)$ sets of equations are compatible under the thermal wind constraint and should provide the same solution. However, due to errors in measurements (instrumentation errors) and computations (truncation errors), the parameter $r^{(k)}$ may vary with m. We have developed an optimization scheme to minimize errors.

If the absolute velocity $(u^{(k)}, v^{(k)})$ is known, we may use the thermal wind relation (10) to obtain the absolute velocity at any level m,

$$\hat{u}^{(m)} = u^{(k)} + \Delta u_{mk}, \quad \hat{v}^{(m)} = v^{(k)} + \Delta v_{mk},$$

$$\hat{w}^{(m)} = -\frac{u^{(m)} \partial\rho^{(m)} / \partial x + v^{(m)} \partial\rho^{(m)} / \partial y}{\partial\rho^{(m)} / \partial z}. \quad (15)$$

The computed $[\hat{u}^{(m)}, \hat{v}^{(m)}, \hat{w}^{(m)}]$ may not be in the same direction as the P-vector $[P_x^{(m)}, P_y^{(m)}, P_z^{(m)}]$ at the level m. If we assume that at the level m, the P-vector exists

$$\frac{|\nabla\rho \times \nabla q|}{|\nabla\rho||\nabla q|} > \varepsilon_1 \quad (16)$$

and that the velocity should parallel the vector $\boldsymbol{P}^{(m)}$, an error can be easily defined by (Fig. 3)

$$E_m = \left| V^{(m)} \mathrm{P}^{(m)} - \hat{\mathrm{v}}^{(m)} \right| = 2\sin\left[\frac{1}{2}\left(\mathrm{P}^{(m)}, \hat{\mathrm{v}}^{(m)}\right)\right] V^{(m)}$$

$$\simeq V^{(m)} \sin\left(\mathrm{P}^{(m)}, \hat{\mathrm{v}}^{(m)}\right), \quad (17)$$

here $V^{(m)} = |\hat{\mathrm{v}}^{(m)}|$, and $(\boldsymbol{P}^{(m)}, \hat{\mathrm{v}}^{(m)})$ is the angle between two vectors $\boldsymbol{P}^{(m)}$ and $\hat{\mathrm{v}}^{(m)}$. The total error of the water column velocity caused by the uncertainty of $(u^{(k)}, v^{(k)})$ is

$$E = \sqrt{\sum_m \left(h_m E_m\right)^2}$$

where h_m is the thickness of the m-th layer (see Table 1). We determine the velocity $(u^{(k)}, v^{(k)})$ such that the total error E becomes minimum, i.e.,

$$\frac{\partial E}{\partial u^{(k)}} = 0, \quad \frac{\partial E}{\partial v^{(k)}} = 0. \quad (18)$$
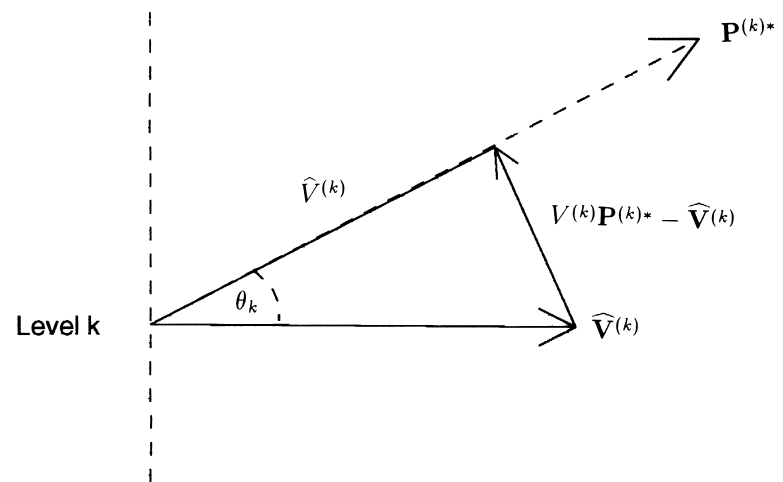

Fig. 3. Error caused by uncertainty of the velocity at the level k.

Table 1. Distribution of vertical levels.

Level	Depth (m) of T, S	Thickness (m)
1	12.5	25.0
2	37.5	25.0
3	70.0	40.0
4	125.0	70.0
5	215.0	110.0
6	370.0	200.0
7	635.0	330.0
8	1025.0	450.0
9	1575.0	650.0
10	2350.0	900.0
11	3250.0	900.0
12	4150.0	900.0

Substitution of (17) into (18) leads to a 2×2 algebraic equations for determining $(u^{(k)}, v^{(k)})$,

$$A_{11}u^{(k)} + A_{12}v^{(k)} = F_1$$

$$A_{21}u^{(k)} + A_{22}v^{(k)} = F_2 \quad (19)$$

where

$$A_{11} = \Sigma_m a_{11}^{(m)}, \quad A_{12} = \Sigma_m a_{12}^{(m)}, \quad A_{21} = A_{12}, \quad A_{22} = \Sigma_m a_{22}^{(m)},$$

$$F_1 = -\Sigma_m\left(a_{11}^{(m)}\Delta u_{mk} + a_{12}^{(m)}\Delta v_{mk}\right),$$

$$F_2 = -\Sigma_m\left(a_{21}^{(m)}\Delta u_{mk} + a_{22}^{(m)}\Delta v_{mk}\right) \quad (20)$$

and

$$a_{11}^{(m)} \equiv \left(P_y^{(m)}\right)^2 f^{(m)}, \quad a_{12}^{(m)} \equiv -P_x^{(m)} P_y^{(m)} f^{(m)},$$

$$a_{22}^{(m)} \equiv \left(P_x^{(m)}\right)^2 f^{(m)},$$

$$f^{(m)} \equiv \left[1 + \left(\frac{\partial \rho^{(m)}/\partial x}{\partial \rho^{(m)}/\partial z}\right)^2 + \left(\frac{\partial \rho^{(m)}/\partial y}{\partial \rho^{(m)}/\partial z}\right)^2\right] h_m^2. \tag{21}$$

The absolute velocity at the level $z = z_k$ can be computed by

$$u^{(k)} = \frac{F_1 A_{22} - F_2 A_{12}}{F_{11} A_{22} - F_{12} A_{21}}, \quad v^{(k)} = \frac{F_2 A_{11} - F_1 A_{21}}{F_{11} A_{22} - F_{12} A_{21}}. \tag{22}$$

Substitution of (21) into (20) makes the second necessary condition (14) into that if

$$A_{11} A_{22} - A_{12} A_{21} = 0 \tag{23}$$

all the inverse methods fails, In other words, the second necessary condition can be written as

$$\left|A_{11} A_{22} - A_{12} A_{21}\right| > \varepsilon_2 \tag{24}$$

there exists β-turning and we may use inverse method to obtain velocity fields.

The P-vector inverse method is essentially the β-spiral method with two necessary conditions. The benefit of using the P-vector method is to filter out those data points.

5. Modular Ocean Model (MOM)

Any inverse method involves two different kinds of errors: observational and modeling errors. The best way to verify the model is to use a no-error data set. Since there is no such data set, we may use a set of steady state solutions from a numerical model as a no-error data set. In this study, we use the steady-state solutions of temperature and salinity from Pacanowski *et al.* (1991) version of the Bryan-Cox-Semtner ocean general circulation model (OGCM), which is based on the work of Bryan (1987). The model domain consists of a 60° square box in latitude-longitude space from 10°–70°N and 10°–75°W. Along the western boundary, an idealized shelf with a structure similar to that in Holland (1973) is included. The horizontal grid spacing is 2° latitude by 2° longitude. The model has 12 levels in the vertical, and the depth distribution is the same as that of Cai (1995) and are listed in Table 1. Values assigned to the various model parameters are listed in Table 2. No-slip and insulating

Table 2. Model coefficients.

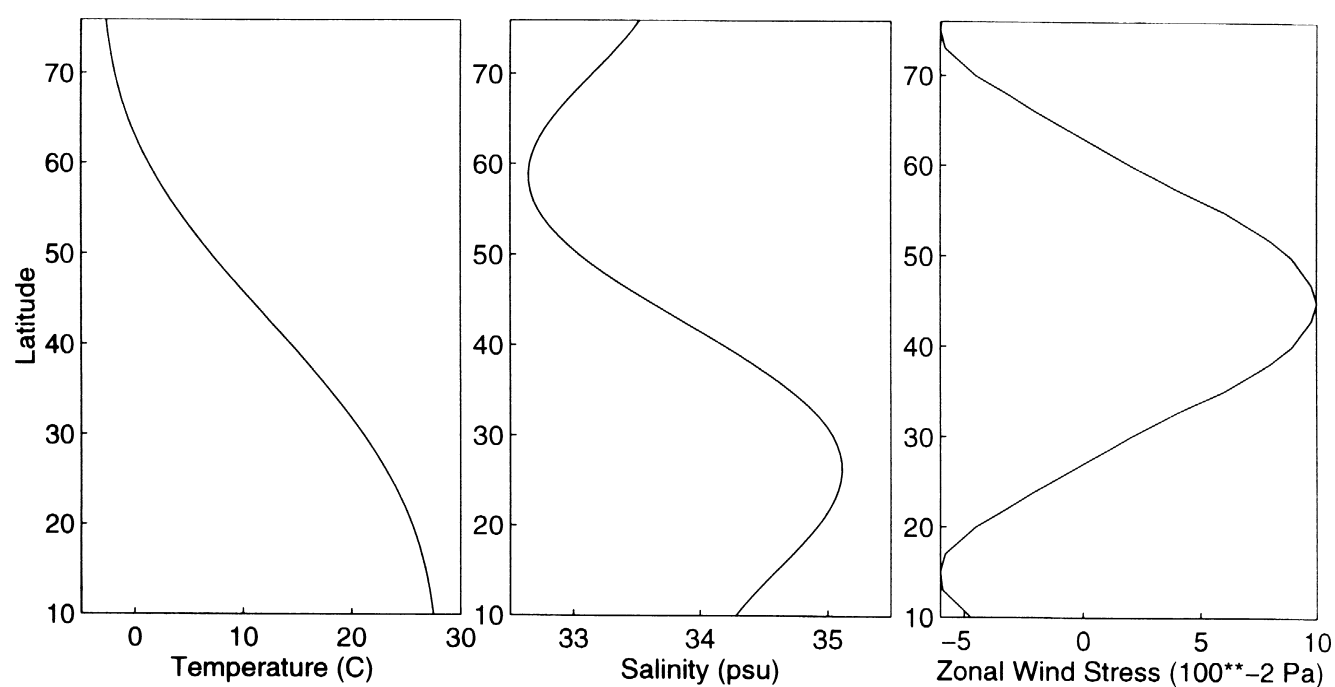| Parameter	Symbol	Value
Horizontal diffusivity	A_{TH}	1×10^3 m^{2}s^{-1}
Horizontal viscosity	A_{MH}	2×10^5 m^{2}s^{-1}
Vertical diffusivity	A_{TV}	1×10^{-4} m^{2}s^{-1}
Vertical viscosity	A_{MV}	1×10^{-4} m^{2}s^{-1}
Characteristic density	ρ_o	1025 kg m^{-3}
Heat capacity	C_w	4×10^3 J kg^{-1}K^{-1}

Fig. 4. Surface boundary conditions. Temperature and salinity profiles used in Haney-type restoring forcing condition and surface wind stress.

boundary conditions are applied at the lateral boundaries. The model uses the Cox (1987) parameterization to compute vertical diffusion and convection implicitly. The enhanced vertical diffusivity in regions of static instability is set at 10^5 cm^{2}s^{-1}, which is the convective adjustment in the model.

The temperature and salinity of upper-most level are relax under a Haney (1971) restoration to a zonally uniform temperature profile:

$$T_a(\varphi) = 30.0 - \frac{33.0}{80.0}\varphi + 4.0\sin\left[\frac{6.283}{75.0}(\varphi - 5.0)\right] \qquad (25)$$
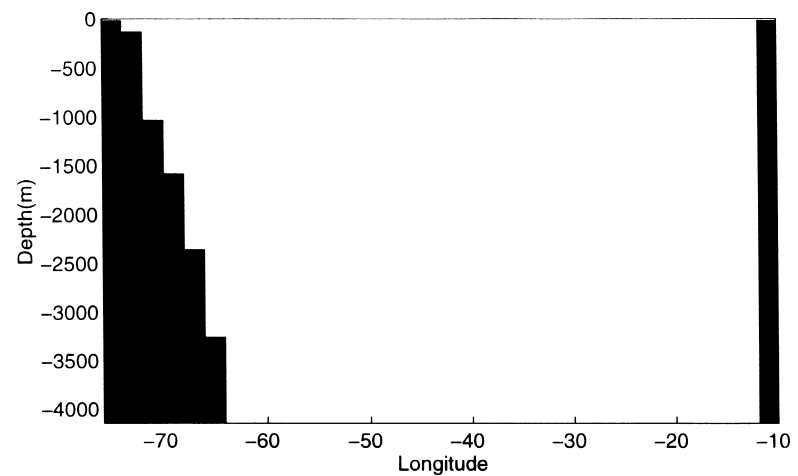
and a salinity profile:

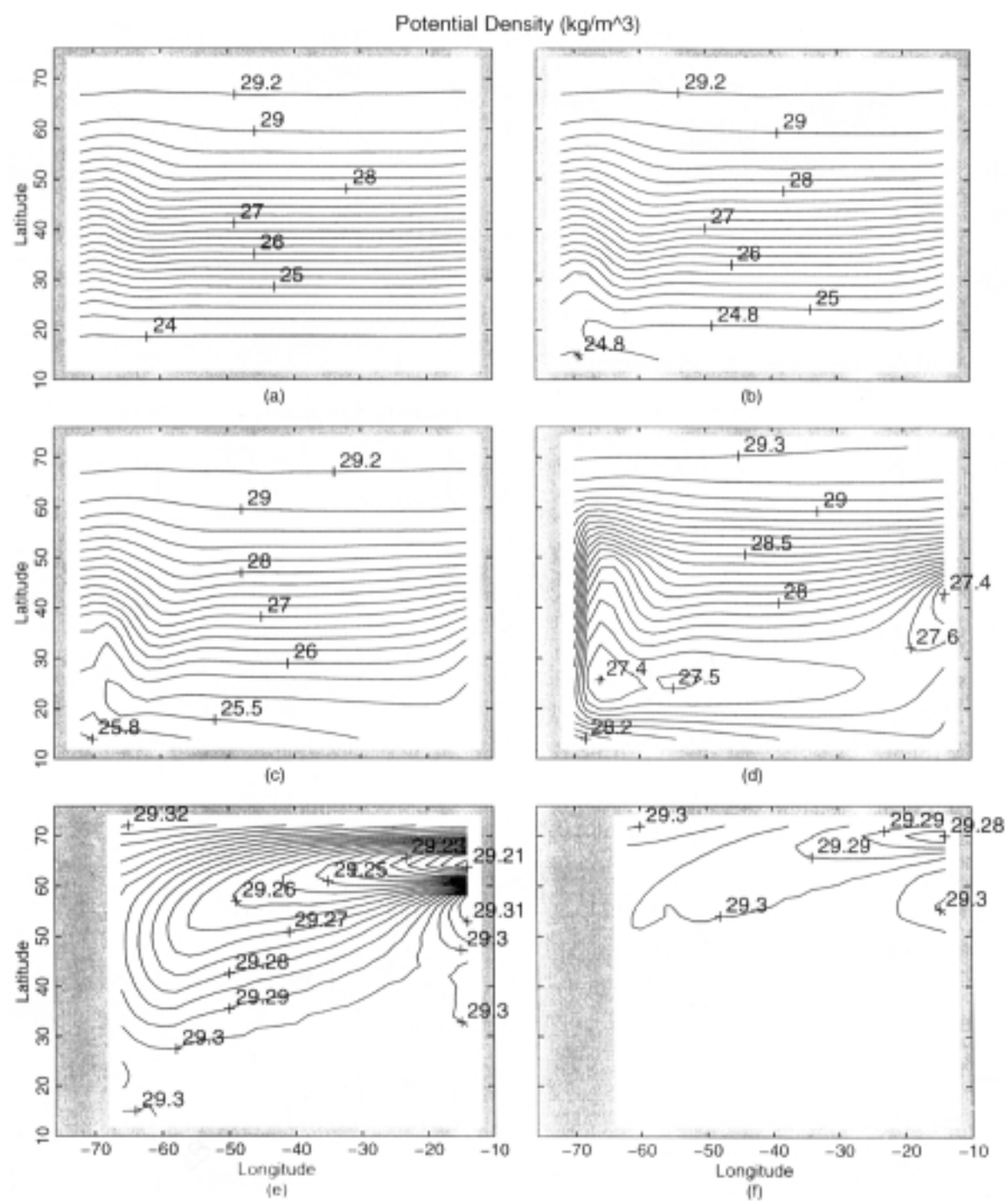Fig. 5. The *x*-dependent bottom topography used in the OGCM.

Fig. 6. Statistically steady potential density (kg/m^3) from the OGCM simulation at different depths: (a) 12.5 m, (b) 37.5 m, (c) 70 m, (d) 215 m, (e) 1,575 m, and (f) 3,250 m.

$$S(\varphi) = 35.0 - \frac{1.32}{50.0}\varphi + 0.84\sin\left[\frac{6.283}{55.0}(\varphi - 15.0)\right] \qquad (26)$$

with a relaxation time-scale of 25 days (over a modeled top mixed 25 m). The model is also subject to the zonal wind stress of Bryan (1987). Figure 4 shows the surface boundary conditions. The bottom topography is assumed only dependent on x, and has a staircase-type change west of 64°W and no change east of 64°W (Fig. 5).

The techniques of Bryan (1987) for acceleration equilibration of the model solution are used. This includes using a longer time step at depth. The acceleration factor increases from 1 at the surface level to 8 at the bottom level. After 750

surface years (6,000 years at the bottom) the model reaches a statistically steady state (total kinetic energy reaches equilibrium).

6. MOM Model Generated Steady-State Data

The MOM model output includes potential temperature (θ), salinity (S), and velocity (u, v, w). The statistically steady potential density field was computed from θ and S fields. Figure 6 shows the σ_θ ($\equiv \rho - 1000$) fields at different depths. The most evident features are listed as follows. The maximum values (29.2–29.3 kg/m^3) appear at the high latitudes (near 70°N) at all depths. The horizontal σ_θ gradient reduces as the depths increases. The low σ_θ water appears at the equatorial region near surface and stretches northward as
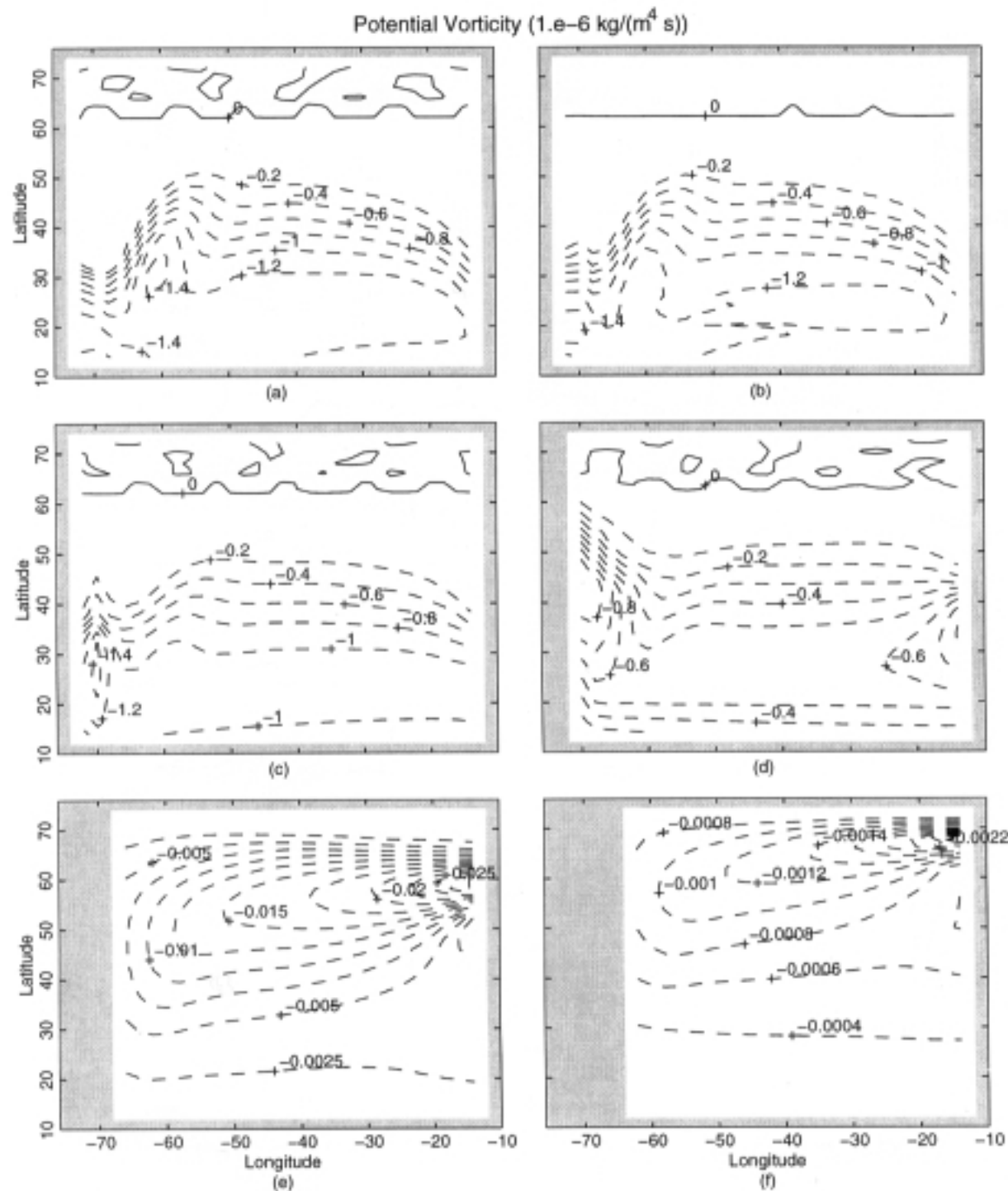

Fig. 7. Statistically steady potential vorticity from the OGCM simulation at different depths: (a) 12.5 m, (b) 37.5 m, (c) 70 m, (d) 215 m, (e) 1,575 m, and (f) 3,250 m.

the depth increases. Near the surface (Fig. 6(a)) the σ_θ curves are almost zonal except at the western boundary, where the σ_θ curves bend towards the north, indicating the northward movement of low σ_θ equatorial water. At the depths of 37.5 m (Fig. 6(b)) and 70 m (Fig. 6(c)), the northward movement of the equatorial low σ_θ water becomes more evident. At the depth of 215 m (Fig. 6(d)), the low σ_θ zone shifts northward. Two centers of low σ_θ (27.4 kg/m^3) are found at the southwest corner (25°N, 74°W) and at the middle of the eastern boundary. At the deep levels (Figs. 6(e) and 6(f)), σ_θ is very uniform. The minimum zone of σ_θ is located at around 60°N.

The statistically steady potential vorticity field (q) was computed from σ_θ. Figure 7 shows the q ($\equiv f\partial\sigma_\theta/\partial z$) field at different depths. The most evident features are listed as follows. The values of q are either negative or zero. There is

an anticyclonic gyre occupying the majority of the domain. In upper levels (12.5 m, 37.5 m, and 70 m), the strongest negative q center (with a value around -1.4×10^{-6} kg m^{-4} s^{-1}) is located near the southwest corner (60°–70°W, 20°–35°N). As depth increases, the magnitude of q-values reduces. The strongest negative q center with values around -2.5×10^{-8} kg m^{-4}s^{-1} at 1,575 m depth and -2.2×10^{-9} kg m^{-4}s^{-1} at 3,250 m depth (2-3 orders of magnitude smaller than the upper levels), is located near the northeast corner (20°–10°W, 55°–65°N).

We may verify the MOM ρ, q data in terms of the two necessary conditions. The vector product of $\nabla\rho$ and ∇q is written by

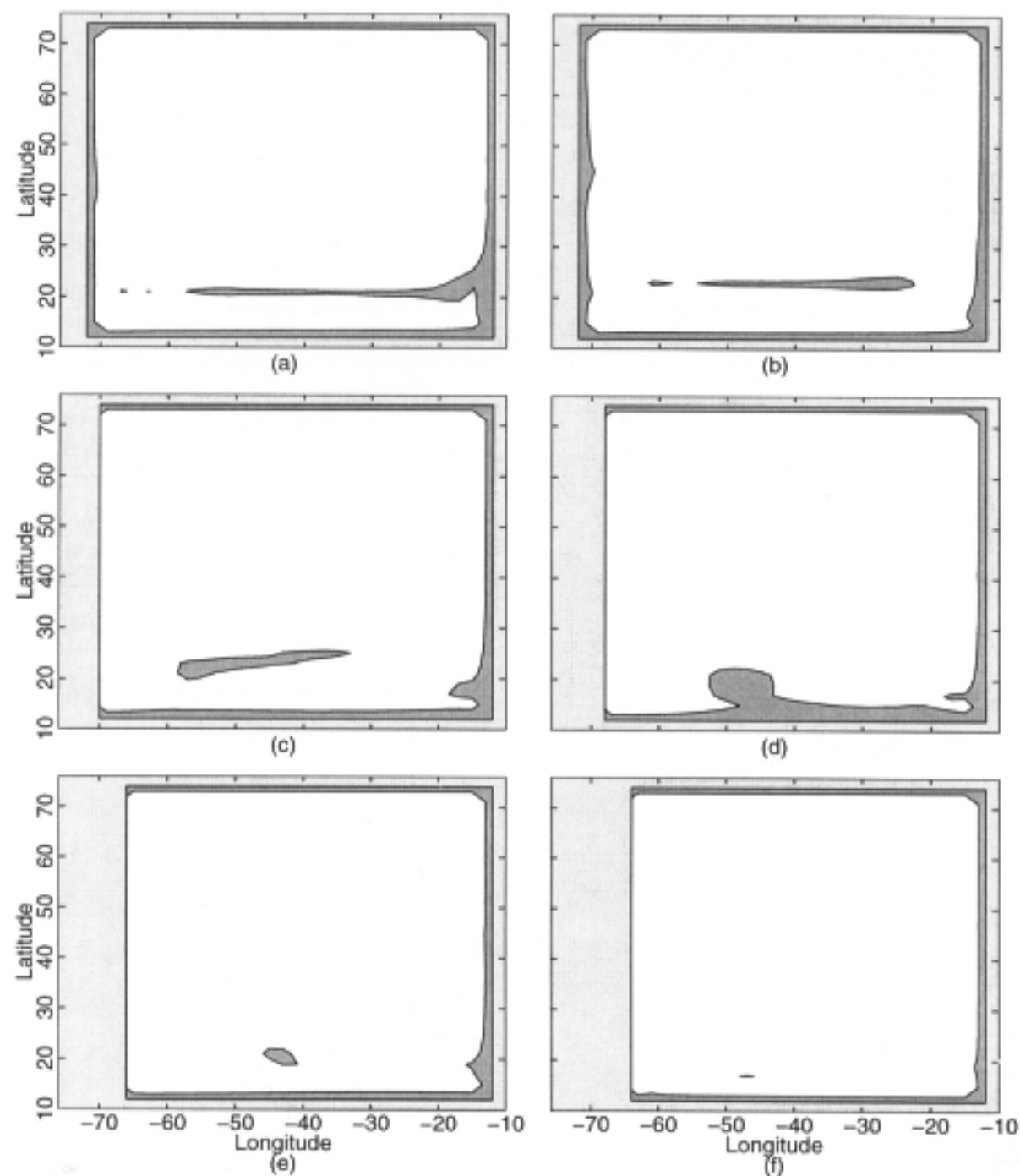$$\nabla\rho \times \nabla q = \boldsymbol{P} \, |\nabla\rho| \, |\nabla q| \sin\delta$$

Fig. 8. Regions with $|\sin\delta| \leq 10^{-5}$ at (a) 370-m, (b) 635-m, (c) 1,025-m, (d) 1,575-m, (e) 2,350-m, and (f) 3,250-m.

where δ is the intersection angle. Since δ cannot be exactly zero when computed from data. A small value was taken as the criterion $\delta_c = 10^{-5}$. If $|\delta| \leq \delta_c$, the ρ surface is thought to be parallel to the q surface. Figure 8 shows the regions at six different depths where the first necessary condition fails.

7. MOM Generated Statistically Steady-State Velocity Field

Figure 9 shows the MOM generated statistically steady horizontal velocities at several depths: (a) 12.5 m, (b) 37.5 m, (c) 70 m, (d) 215 m, (e) 1575 m, (f) 3250 m. The circulation patterns can be outlined as follows. Westward-moving equatorial currents are evident in upper levels ($z \geq -215$ m) and disappear in the deeper layer ($z < -215$ m). The

width of the upper layer equatorial current is around 6° in latitude. When the upper layer equatorial current approaches the western boundary, it turns direction and becomes the western boundary current. The maximum velocity of the western boundary current reaches 13 cm/s. The intermediate level (1,575 m) and deep level (3,250 m) feature a westward current originating at the northeast corner. This current turns southwestward at around 50°W and branches into two western boundary currents (northward and southward) as approaching the western boundary. The bifurcation is found at 40°N for the depth of 1,575 m, and at 60°N for the depth of 3,250 m. The deep currents are weak (≤ 2 cm/s).

The velocity spiral can be identified for each grid point by the plot of V_h of all the depths (Fig. 10). There are 12
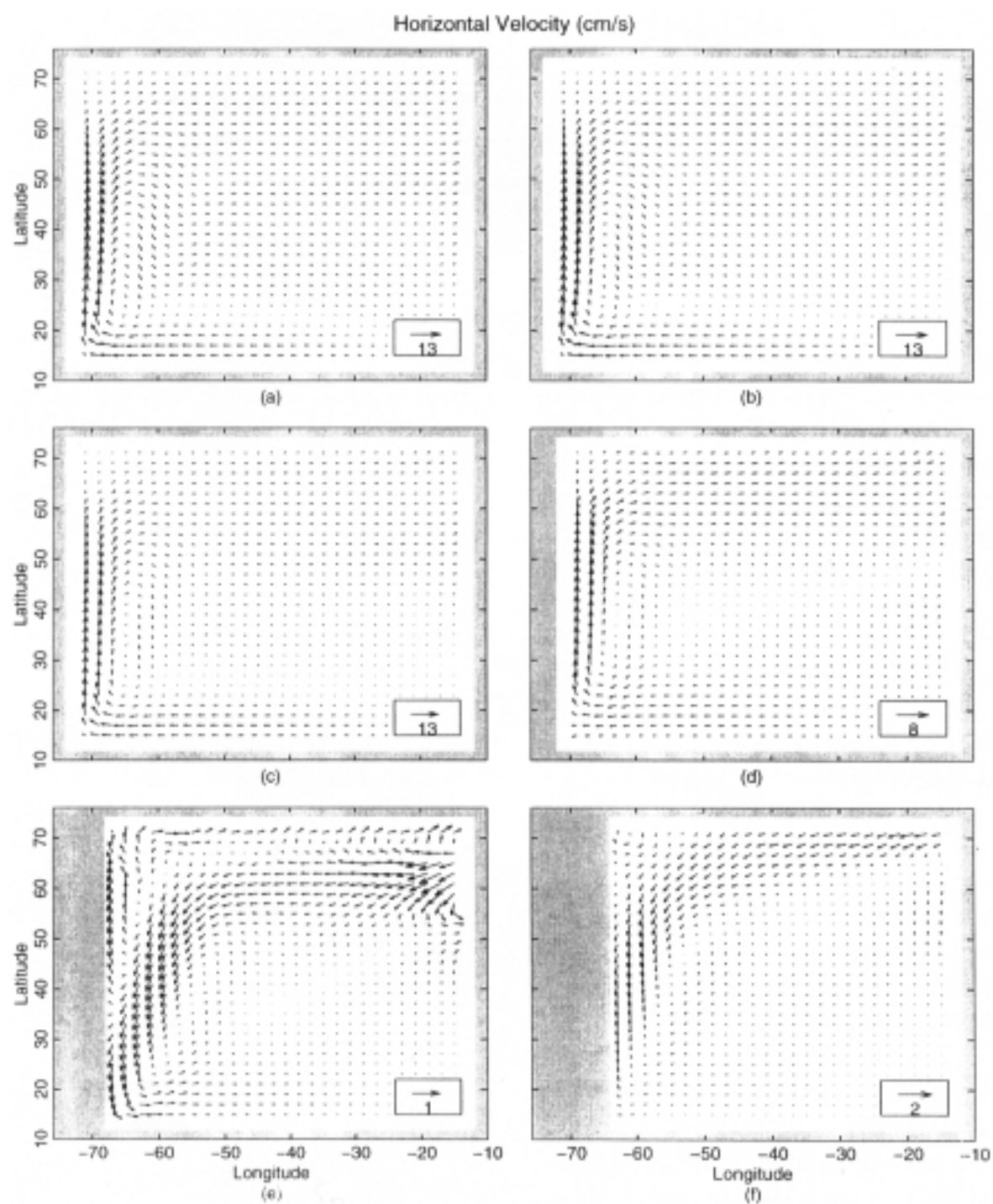

Fig. 9. Statistically steady velocity from the OGCM simulation at different depths: (a) 12.5 m, (b) 37.5 m, (c) 70 m, (d) 215 m, (e) 1,575 m, and (f) 3,250 m.
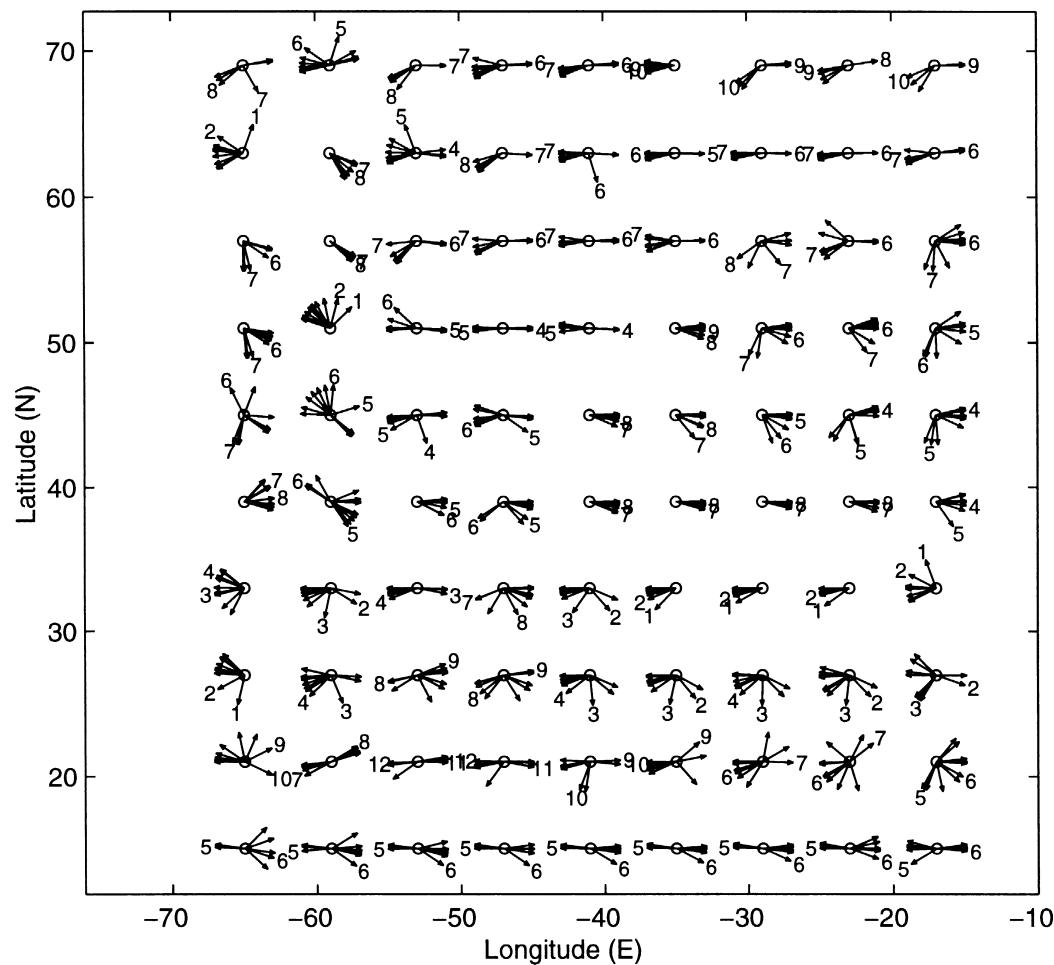
Fig. 10. Velocity spirals of V_h (12 vectors at each grid). Two numbers given at each grid indicate the maximum turning between two consecutive levels.

vectors at each grid. Coincidence of the vectors means no β-turning. Two numbers given at each grid indicate the maximum β-turning between two consecutive levels such as from 370-m (level 6) to 635-m (level 7) in the sub-tropical regions (10°–30°N) and from 1025-m (level 8) to 1575-m (level 9) in the mid- and high-latitudes (north of 40°N). At some locations, the maximum turning occurs at deeper levels. Usually, strong vertical turning of the horizontal velocity indicates a strong baroclinicity.

8. Absolute Velocities Obtained from the P-Vector Inverse Method Using MOM T, S Output

Taking the statistically steady potential temperature and salinity fields as no-error data sets, we employed the P-vector inverse method to obtain the 3-D absolute geostrophic velocity (u_I, v_I). Figure 11 shows the vector plots of the horizontal velocities at several different depths: (a) 12.5 m, (b) 37.5 m, (c) 70 m, (d) 215 m, (e) 1575 m, (f) 3250 m. The circulation patterns are very similar to the MOM statistically steady-state velocity fields in the upper four levels (12.5 m, 37.5 m, 70 m, and 215 m). The circulation patterns can be outlined as follows. Westward-moving equatorial currents are evident with a width of 6° in latitude. When the equatorial current approaches the western boundary, it turns direction and become the western boundary current. The current velocities are similar at the three levels: 12.5 m, 37.5 m, and

70 m, but weaker in the P-vector inverse method. The lower level (1575 m, and 3250 m) velocity fields are very weak. The major difference between the MOM and the inverse solutions is the western boundary flow bifurcation. The MOM model shows the high latitude westward flow bifurcated at 40°N for the depth of 1,575 m, and at 60°N for the depth of 3,250 m into two western boundary currents (northward and southward). However, the P-vector inverse model does not show this bifurcation.

9. Comparison between Non-Divergent Portions of Two Flow Fields

Given that the MOM model flow field derives from primitive equation dynamics, we don't expect that the velocity fields from the P-vector method (assuming geostrophic dynamics) should match the MOM model velocity fields. The only valid comparison should be with the nondivergent portion of the flow field, i.e.,

$$\nabla^2 \psi_{\text{MOM}} = \frac{\partial\left(f v_{\text{MOM}}\right)}{\partial x} - \frac{\partial\left(f u_{\text{MOM}}\right)}{\partial y},$$

$$\nabla^2 \psi_I = \frac{\partial\left(f v_I\right)}{\partial x} - \frac{\partial\left(f u_I\right)}{\partial y}. \tag{27}$$
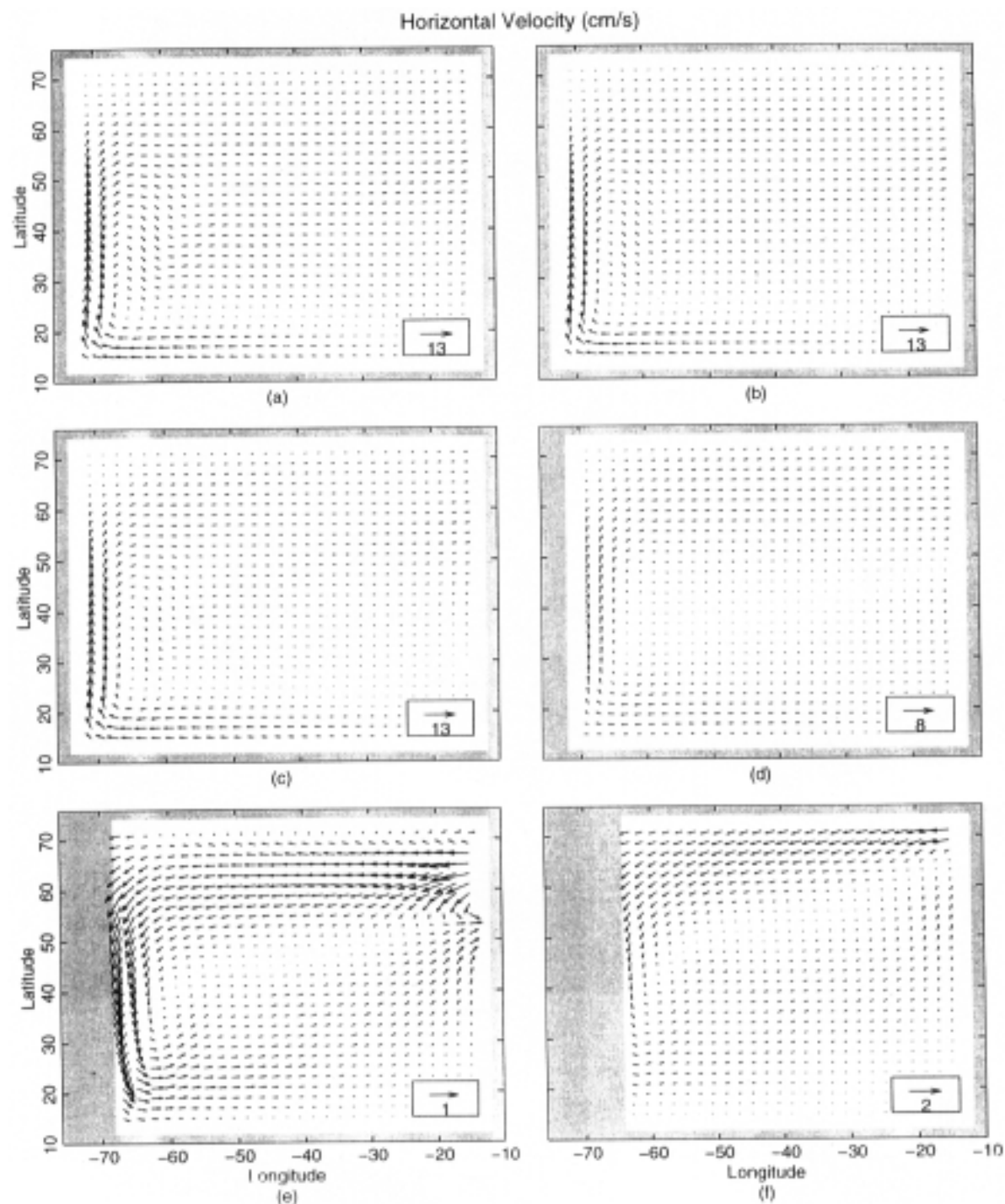
Fig. 11. Absolute velocity fields computed by the P-vector method at different depths: (a) 12.5 m, (b) 37.5 m, (c) 70 m, (d) 215 m, (e) 1,575 m, and (f) 3,250 m.

We solved the two Poisson Equations in (27) by taking (u_{MOM}, v_{MOM}), (u_I, v_I) as forcing functions under the boundary conditions

$$\psi_{MOM}\big|_\Gamma = 0, \quad \psi_I\big|_\Gamma = 0 \quad (28)$$

where Γ represents the lateral boundaries, and $\boldsymbol{n}$ denotes the outgoing normal direction.

The ψ_{MOM} field has the following features (Fig. 12): a nearly basin-wide anticyclonic gyre in the upper levels (12.5 m, 37.5 m, 70 m, and 215 m) and a nearly basin-wide cyclonic gyre in the lower levels (1575 m, 3250 m). These gyres are evident by closed ψ_{MOM} contours with a maximum

value for the anticyclonic gyre and with a minimum value for the cyclonic gyre. Both basin-wide gyres are asymmetric. The center of the gyres (both upper and lower levels) is towards the west, with a strong western boundary current. In the upper levels, a weak and narrow cyclonic gyre appears in the high latitudes (north of 60°N) east of 55°W (south of Greenland and Iceland.) This weak high latitude cyclonic gyre reduces its size with depth and becomes an anticyclonic gyre which stretches westward to the western boundary in the intermediate level (1,575 m). In the deep level (3,250 m), the cyclonic gyre fills the whole basin.

The streamfunction ψ_I (Fig. 13) at the six different depths shows that the pattern of the two fields are quite similar: a nearly basin-wide anticyclonic gyre in the upper
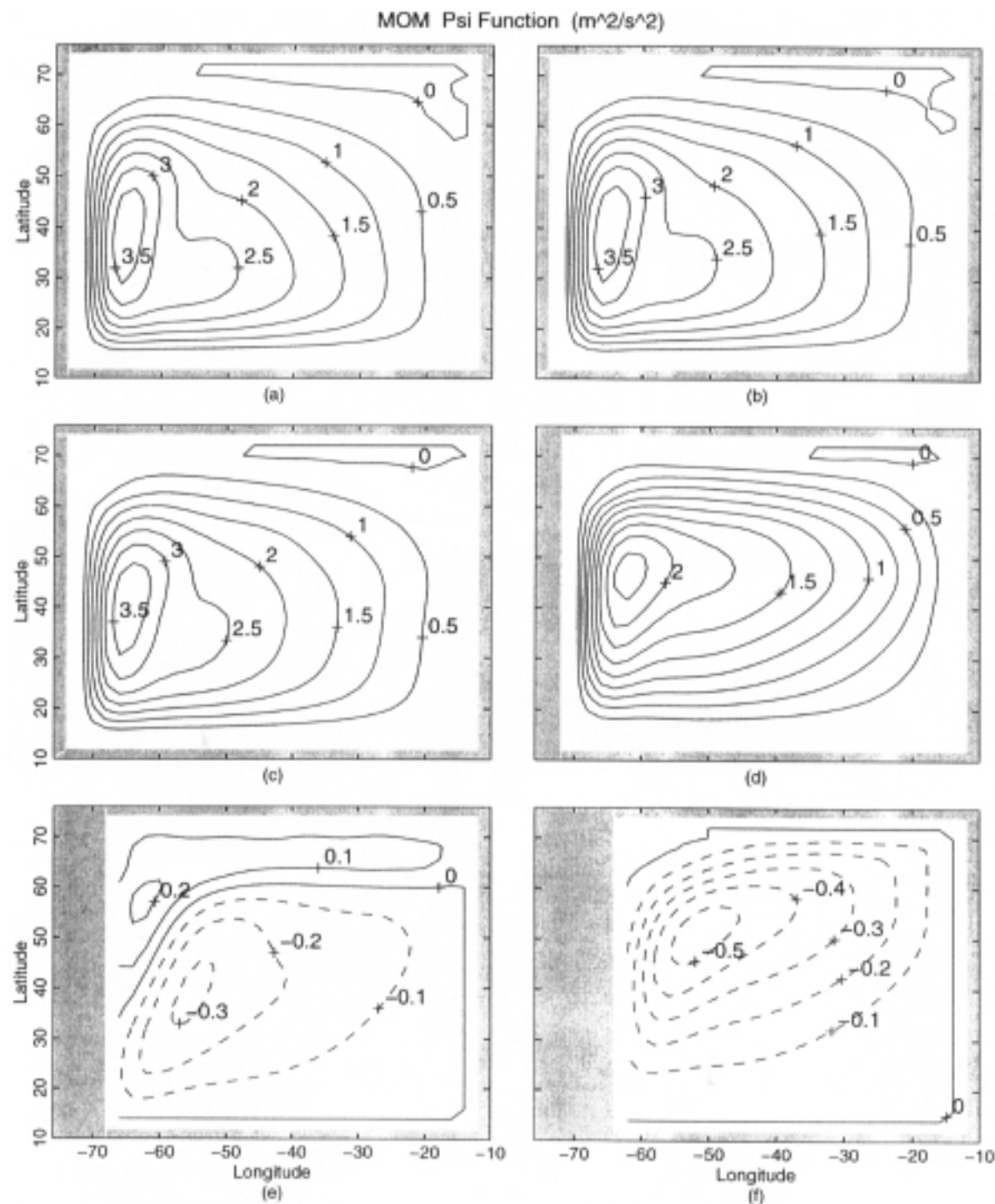
MOM Psi Function (m^2/s^2)

Fig. 12. Horizontal distributions of ψ_{MOM} at different depths: (a) 12.5 m, (b) 37.5 m, (c) 70 m, (d) 215 m, (e) 1,575 m, and (f) 3,250 m.

levels (12.5 m, 37.5 m, 70 m, and 215 m) and a nearly basin-wide cyclonic gyre in the lower levels (1575 m, 3250 m). These gyres are featured by closed ψ_I contours with a maximum value for the anticyclonic gyre and with a minimum value for the cyclonic gyre. The center of the basin-wide gyres (both upper and lower levels) is towards the west, and has a strong western boundary current. The patterns are very similar between ψ_{MOM} and ψ_I at all depths. The difference between ψ_{MOM} and ψ_I are: (a) the nearly basin-wide gyre is stronger in the MOM model than in this P-vector model except for the intermediate level (1,575 m), where the cyclonic gyre obtained by the β-vector model is stronger; (b) in the upper levels (12.5 m, 37.5 m, 70 m, and 215 m) the high latitude (north of 60°N) cyclonic gyre obtained by the

P-vector model stretches from the eastern boundary to the western boundary; (c) in the intermediate level (1,575 m), the high latitude anticyclonic gyre by the P-vector model is located in the eastern part (east of 40°W) rather than stretching to the western boundary in the MOM model.

Relative difference (I_ψ) between two streamfunctions (ψ_{MOM} and ψ_I) for each level can be depicted by a ratio between root-mean-square (RMS) difference and standard deviation of MOM results ($\sigma_{\psi_{MOM}}$),

$$I_\psi = \frac{\sqrt{\dfrac{1}{M-1}\sum\left(\psi_{MOM} - \psi_I\right)^2}}{\sigma_{\psi_{MOM}}},$$
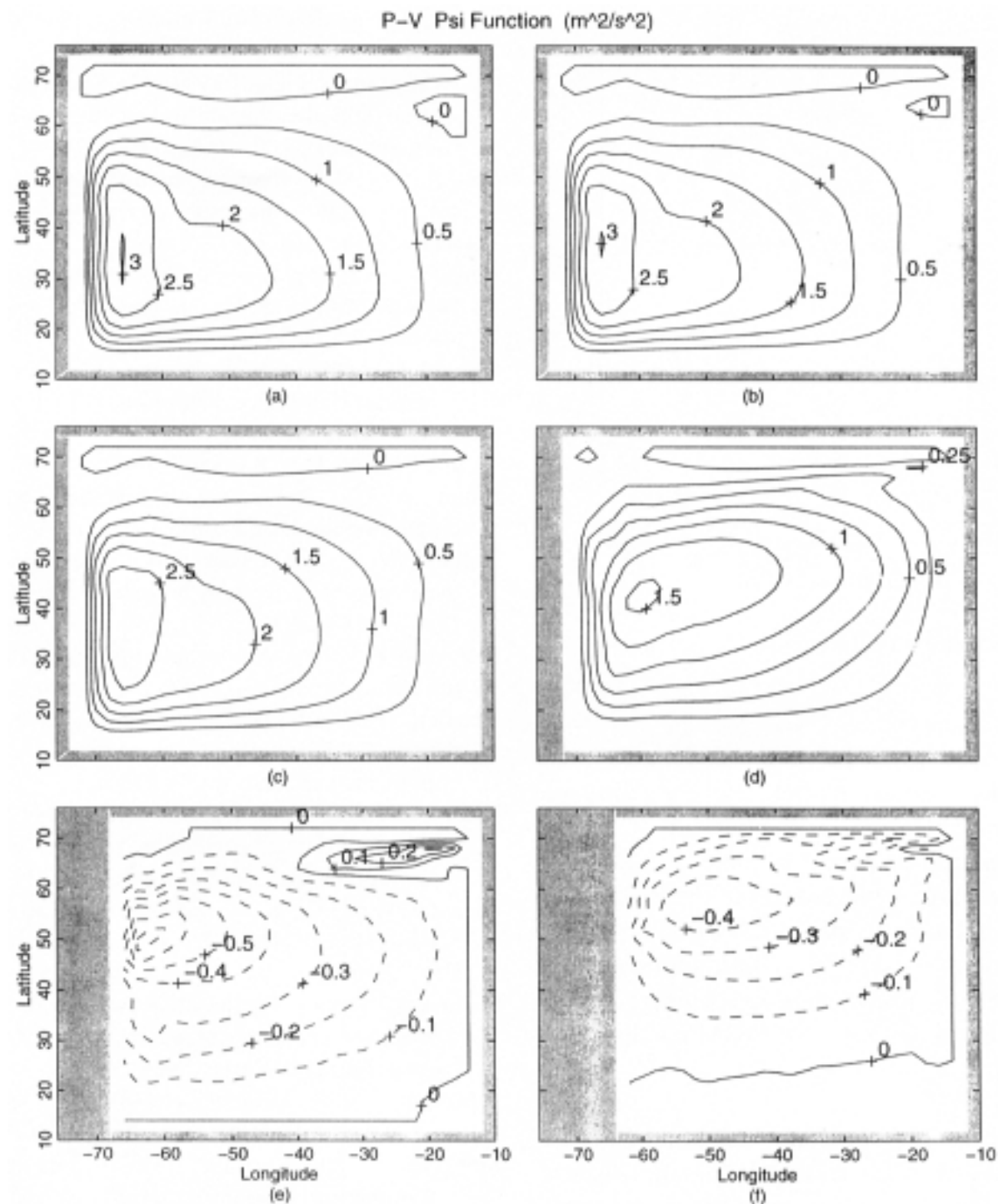
Fig. 13. Horizontal distributions of ψ_I at different depths: (a) 12.5 m, (b) 37.5 m, (c) 70 m, (d) 215 m, (e) 1,575 m, and (f) 3,250 m.

$$\sigma_{\psi_{\text{MOM}}} = \sqrt{\frac{1}{M-1}\sum\left(\psi_{\text{MOM}} - \overline{\psi_{\text{MOM}}}\right)^2}. \qquad (29)$$

Here M is the total number of the horizontal grid points. The numerator and denominator of (29) show the mean difference between two streamfunctions and the variability of ψ_{MOM}, respectively. The smaller the I_ψ, the smaller the difference between the inverse method and MOM solutions. Near surface, I_ψ is small (≈ 0.15), increases with depth until 1000 m (level 8) with the maximum value of 0.8, and then decrease with depth (Fig. 14). In deep levels ($z \leq -2,500$ m), I_ψ reduces with depth from 0.3 to 0.2. Near bottom, I_ψ is around 0.2. The maximum value of I_ψ may caused by strong baroclinicity near that level (Fig. 9).

10. Conclusions

(1) Two necessary conditions were discussed in this paper for the validity of any inverse method. They are (a) non-coincidence of potential density and potential vorticity surfaces; and (b) β-turning. The P-vector concept provides a logical way of checking these two conditions. Existence of the P-Vector guarantees the satisfaction of the first necessary condition. Existence of vertical turning in the horizontal P-Vector components, $\boldsymbol{P}_h = (P_x, P_y)$, guarantees the satisfaction of the second necessary condition.

(2) The P-vector inverse method with pre-required conditions was evaluated using the MOM model. The statistically steady solutions of temperature and salinity from MOM are used as a no-error data set for computing absolute geostrophic velocities by the P-vector inverse method.
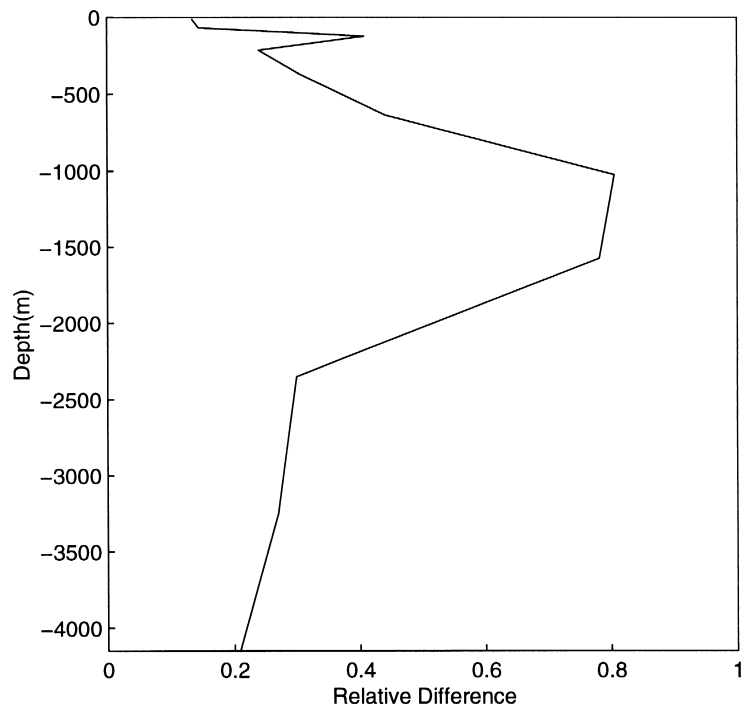
Evaluation of P-Vector Method   197

Fig. 14. Vertical variation of the relative difference I_ψ.

Similarity of ψ_{MOM} and ψ_I fields is found at different depths and confirms that the inverse method has capability of picking up the major signal of the velocity field.

(3) The introduction of P-vector makes the β-spiral formulation analytical and simple. However, the P-vector is calculated by differentiation of potential vorticity which may suffer from various noises. The continuation of this study should include the β-spiral method and compare among P-vector method, β-spiral method, and MOM results.

Acknowledgements

References

Behringer, D. W. and H. Stommel (1980): The beta spiral in the North Atlantic subtropical gyre. *Deep Sea Res.*, **27A**, 225–238.

Bryan, K. (1987): Parameter sensitivity of primitive equation ocean general circulation models. *J. Phys. Oceanogr.*, **17**, 970–985.

Cai, Wenju and S. J. Godfrey (1995): Surface heat flux parameterization and the variability of thermocline circulation. *J. Geophys. Res.*, **100**, 10,679–10,692.

Chu, P. C. (1994): P-vector method for determining ocean circulation from hydrographic data. *Ocean Modeling*, **104**, unpublished manuscript.

Chu, P. C. (1995): P-vector method for determining absolute velocity from hydrographic data. *Marine Technology Society Journal*, **29**(3), 3–14.

Cox, M. D. (1987): GFDL *Ocean Model Circular No. 7*. GFDL/Princeton University, Princeton, N.J., 1 pp.

Davis, R. (1978): On estimating velocity from hydrographic data. *J. Geophys. Res.*, **83**, 5507–5509.

Haney, R. L. (1971): Surface boundary condition for ocean circulation models. *J. Phys. Oceanogr.*, **1**, 241–248.

Holland, W. R. (1973): Baroclinic and topographic influences on the transport in western boundary currents. *Geophys. Fluid Dyn.*, **4**, 187–210.

Killworth, P. (1986): A Bernoulli inverse method for determining the ocean circulation. *J. Phys. Oceanogr.*, **16**, 2031–2051.

Needler, G. T. (1982): On determining the velocity from the density field-including a closed form. *Ocean Modelling*, **46**, unpublished manuscript.

Olbers, D. J., M. Wenzel and J. Willbrand (1985): The inference of North Atlantic circulation patterns from climatological hydrographic data. *Rev. Geophys.*, **23**, 313–356.

Pacanowski, R. C., K. W. Dixon and A. Rosati (1991): GFDL Modular Ocean Model, Users Guide Version 1.0, GFDL Tech. Rep., 2, 46 pp.

Pedlosky, J. (1986): Thermocline theories. p. 55–101. In *General Circulation of the Ocean*, ed. by H. G. I. Abardanel and W. R. Young, Springer-Verlag, New York.

Schott, F. and H. Stommel (1978): Beta spirals and absolute velocities in different oceans. *Deep Sea Res.*, **25**, 961–1010.

Stommel, H. and F. Schott (1977): The beta spiral and the determination of the absolute velocity field from hydrographic station data. *Deep Sea Res.*, **24**, 325–329.

Wunsch, C. (1978): The general circulation of the North Atlantic west of 50°W determined from inverse method. *Rev. Geophys.*, **16**, 583–620.

Wunsch, C. and B. Grant (1982): Towards the general circulation of the North Atlantic Ocean. *Prog. Oceang.*, **11**, 1–59.